TIME-DEPENDENT TENSILE BEHAVIOR OF SLAG-BASED ALKALI ACTIVIATED CONCRETE

H.J. BEZEMER[*], S. MUSTAFA[*] AND M. LUKOVIĆ[*]

[*] Delft University of Technology, Department of Engineering Structures
Stevinweg 1, 2628CN Delft, The Netherlands
e-mail: H.J.Bezemer@tudelft.nl

Key words: Alkali Activated Concrete, Tensile Strength, Fracture Energy, Drying, Time-dependency

Abstract: With the development and use of Alkali Activated Concretes (AACs), a more sustainable alternative to Portland Cement Concretes (PCCs), it is becoming ever more important to understand its mechanical behavior over time. Herein, tensile behavior of a slag-based AAC (S-AAC) was investigated on dog-bone shaped samples tested in direct tension and compared to a CEMIII/B-based concrete (S-PCC). Samples have been fog-cured for 28 days and successively exposed to 55% relative humidity and 20ºC until testing, at testing ages 28 days, 3 months, 6 months and 1 year. Stress-strain behavior of S-AAC was characterized by a significantly lower tensile strength and elastic modulus than S-PCC. From 28 days to 3 months, both concretes showed a reduction in tensile strength, which partially recovered at 6 months. Interestingly, after partial recovery, both concretes showed reduced tensile strength at the age of 1 year. Stress-crack opening curves and development of characteristic length over time showed that, unlike S-PCC, S-AAC softens under drying, which might be an effect of shrinkage-induced microcracking in S-AAC.

1 INTRODUCTION

In recent years, sustainability has gained significant attention and industries are challenged to reduce their carbon footprint. The concrete industry is responsible for 5-8% of the anthropogenic carbon emissions [1-3], mainly due to ordinary Portland cement (OPC) production. One way to reduce these emissions is by (partially) replacing OPC by industrial by-products, such as ground granulated blast furnace slag (GGBFS). Full replacement of cement can be realized by alkali activation of GGBFS [4, 5]. Although alkali activated concretes (AACs) are promising, their wider application is hampered by lacking knowledge on their long-term behavior.

In particular, GGBFS-based AACs have been reported to show decreasing mechanical properties over time [6-13], which was attributed to shrinkage-induced microcracking [7, 10, 13-15] and drying-induced chemical changes [14, 16]. However, these studies did not consider the stress-strain behavior, nor did they provide detailed insight into fracture mechanisms. Both could provide further insight in the long-term behavior of AACs and are essential for the development of models. So far, only a few studies have addressed the stress-strain behavior of alkali activated concretes. Thomas et al. [17] investigated the stress-strain behavior of GGBFS-based AACs under compression at 28 days and reported that the ascending branch of the stress-strain curve was similar to OPC-based concrete (OPCC). The post-peak behavior of GGBFS-based AAC was more brittle than that of OPCC, which was attributed to microcracking of AAC. Similar trends were observed by others [18-20], indicating that, like with OPCCs, increasing the strength class of GGBFS-based AACs leads to a more brittle material. Farhan et al. [18] investigated the tensile stress-strain behavior from notched prisms, which were clamped by

an embedded rod. Although they could not capture the post-peak behavior, their GGBFS-based AAC achieved similar tensile strength, higher strain capacity and lower elastic modulus than OPCC at 28 days. To the authors knowledge, no studies have investigated the stress-strain and fracture behavior under tension of GGBFS-based AAC over time, while its necessity is stressed by the sensitivity of GGBFS-based AACs to drying.

The aim of the current study is to investigate the long-term tensile behavior of GGBFS-based AAC. Uniaxial tensile tests have been performed on dogbone-shaped specimens at different ages, reaching up to 1 year. A CEMIII/B-based concrete of a same strength class was tested for comparison. Both concretes are fog-cured for 28 days and successively exposed to drying. Stress-strain behavior and stress-crack opening as well as elastic tensile modulus, non-linearity using a plasticity index, characteristic length and fracture energy are compared for the two concrete mixes at different testing ages.

2 MATERIALS AND METHODS

2.1 Materials

Table 1 shows the mix designs of the studied GGBFS-based Alkali Activated Concrete (denoted as S-AAC) and its reference CEM III/B-based concrete (denoted as S-PCC). The concretes are designed to have comparable aggregate content, aggregate distribution, water-to-solid ratio and compressive strength at 28 days. The specific gravities of GGBFS and CEM III/B are 2890 kg/m^3 and 2950 kg/m^3, respectively. S-AAC is activated by an alkaline solution, which is made by mixing a sodium hydroxide solution (4M) and a sodium silicate solution (27.5 percentage by weight (wt.%) SiO$_2$, 8.25 wt.% Na$_2$O and 64.25 wt.% H$_2$O) in a 1:2.2 weight proportion. The resulting solution has a Na$_2$O concentration of 4.5 wt.% and a silica modulus (n = SiO$_2$/Na$_2$O) of 0.95. The alkaline solution is prepared 24 hours prior to casting. S-PCC is made with water. No admixtures were used.

To verify the comparability of the concretes,

the mean compressive strength at 28 days was determined on a triplicate of 150 mm cubes, following EN-12390-3 [21]. The mean compressive strengths at 28 days reached 69 (±1) MPa and 68 (±2) MPa for S-AAC and S-PCC, respectively.

Table 1: Mix designs

Ingredient	S-AAC (kg/m^3)	S-PCC (kg/m^3)
GGBFS	400	0
CEMIII/B 42.5 N	0	426
Sand (0-4 mm)	787	787
Gravel (4-16 mm)	947	947
Activating solution	200	165
w/s-ratio	0.38	0.38

2.2 Uniaxial tensile testing

For each mixture, quartets of dogbone-shaped specimens (Figure 1) were cast. After casting, the specimens were vibrated on a vibration table and then covered with a plastic film. The specimens were demolded 1 day after casting, placed in a fog chamber (~95% relative humidity (RH) and 20 ºC) for 28 days and successively exposed to 55% RH and 20 ºC until testing. Both concretes were tested at 28 days, 3 months, 6 months and 1 year.

Figure 1 shows the dimensions of the dogbone specimens. The neck of the specimens was 60 x 60 mm^2, which is surpassing 3.5 times the maximum aggregate size of the studied concretes, ensuring a representative cross-section. The height of the specimen was 210 mm (< 4 times width of neck), which is to limit bending effects and ensure uniform crack opening [22]. Furthermore, a 25 mm radial transition is adopted to minimize stress concentrations from the head to the neck of the specimen, following [23].

Testing of the dogbone-shaped specimens was done by gluing the specimens into a specially designed testing rig (Figure 1) under 0.2 MPa pressure. To ensure uniform stress distribution and limit non-uniform crack opening over the cross section of the samples, the testing rig was designed with non-rotating loading platens. These fixed boundary conditions are obtained by a guiding system on the top and four 50 kN load cells on the bottom.
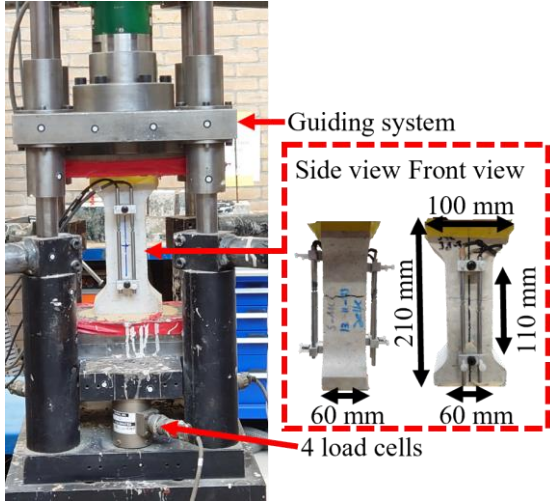
Figure 1: Testing rig and specimen dimensions

The four load cells at the bottom (and weight of the sample) lead to a non-zero force prior to testing, which complicates the determination of zero-force at the beginning of the test. Therefore, zero force was determined at the end of the experiment when the crack opening reaches 1.5 mm, which is when it can be assumed that the crack will no longer transfer stresses [22]. Each side surface of a specimen was instrumented with a set of 2 linear variable differential transformers (LVDTs). One ranging 110 mm, the other 140 mm (Figure 1). The latter was used to control the loading rate under strain-controlled loading. Specimens that failed outside the neck were omitted. Figure 2 shows a typical test result for all four LVDTs. The stress-deformation curve is separated into pre-peak and post-peak behavior, where pre-peak behavior is presented as a stress-strain curve and post-peak as a stress-crack opening curve. Crack opening (CO) is determined by considering elastic and plastic deformations within the measuring length, following **Eq. (1)** [22],

$$CO = L - \frac{\sigma_{ct}}{E} l_{meas} \qquad (1)$$

in which L is the deformation measurement, σ_{ct} is cross-sectional average stress, E is the secant stiffness at peak stress and l_{meas} is the measuring length of a LVDT. The average strain reading of all four LVDTs was used to determine elongation and crack opening.

For every quartet of specimens, the first one

was loaded to failure using a loading rate of 3.7 µm/m/s. The second to fourth specimen was three times loaded from 10-33% of its tensile strength, determined from the first tested sample, using a loading rate of 0.1 MPa/s and successively loaded to failure at 3.7 µm/m/s. Note, strength and stiffness did not tend to differ between monotonic (first sample) and cyclic loaded samples (second to fourth sample). This is in line with earlier findings [24].

Elastic tensile modulus is determined from the third loading cycle, similar to EN 12390-13 [25]. Non-linearity of stress-strain behavior of concrete is assessed with a plasticity index (*PI*) [26], following Equation (2),

$$PI = \frac{\varepsilon_{total}\text{-}E_{ct}f_{ct}}{\varepsilon_{total}} \qquad (2)$$

in which ε_{total} is the total strain of concrete corresponding to peak stress, E_{ct} is the elastic modulus and f_{ct} is the peak tensile stress. Characteristic length (L_{ch}) is determined, following Equation (3) [27],

$$L_{ch} = \frac{E_{ct}G_f}{f_{ct}^2} \qquad (3)$$

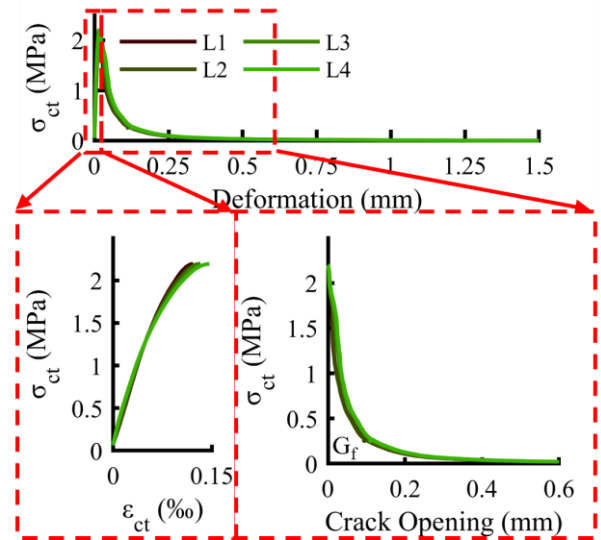in which G_f is the fracture energy, determined from the stress-crack opening curve (Figure 2).

Figure 2: Separation of stress-deformation curve into stress-strain and stress-crack opening up to 0.6 mm crack opening.

3 RESULTS & DISCUSSION

3.1 Stress-strain behavior

Figure 3 shows the stress-strain response for S-AAC and S-PCC tested at different ages. These graphs show that, although having a similar compressive strength, S-AAC has a 28% lower tensile strength than S-PCC at 28 days. This is in line with earlier findings on flexural and tensile splitting strength of GGBFS-based AACs [12, 14, 15, 28, 29] and has been attributed to autogenous shrinkage induced microcracking [30, 31]. As GGBFS-based AACs exhibit up to 12 times larger autogenous shrinkage than PCCs [12, 29, 32, 33], local restraint by aggregates causes tensile stresses and possibly microcracking.

Over time, both concretes show a decrease in tensile strength (Figure 4a). From 28 days to 3 months, tensile strength reduces with 0.83 MPa (20%) and 0.84 MPa (28%) for S-PCC and S-AAC, respectively, and (partially) recovers at 6 months. A temporary reduction of tensile strength of concrete exposed to drying has been observed before [22, 34, 35] and was attributed to the development of eigen stresses. These eigen stresses reduce over time due to relaxation and lead to (partial) recovery of tensile strength. However, the recovery of strength might be limited if eigen stresses lead to microcracking [34]. For S-AAC, the apparent tensile strength at 6 months is 0.48 MPa (16%) lower than its

28 day-value, which is similar to the 0.34 MPa (8%) reduction for S-PCC. Upon visual inspection of the non-casted surfaces, surface cracks were observed for both concretes. Interestingly, after partial recovery of the tensile strength at 6 months, both concretes show a decline in tensile strength from 6 months to 1 year. For GGBFS-based AACs, reduced tensile strength at later ages have been observed before [7, 13, 14] and were attributed to microcracking [7] and drying-induced chemical changes in C-A-S-H-gels [14, 16, 32]. Although aggregate restraint can also cause drying-induced microcracking in CEMI-based concretes [36-38], tensile strength usually tends to increase over time [14, 22, 35] due to continued cement hydration [39]. Yet, S-PCC, a CEMIII/B-based concrete, shows long-term strength reduction, similar to S-AAC.

The strain capacity of S-AAC increased over time, while that of S-PCC reduced (Figure 4b). Note, despite the significant scatter in strain capacity, which is common for uniaxial tensile testing and to some extent intrinsically related to the heterogeneity of concrete, general trends could still be observed. The increase in strain capacity of S-AAC over time could be an effect of 1) reduced elastic modulus (Figure 4c) and 2) propagating and widening of microcracks. Maruyama et al. [36] found that concrete strength is affected by the formation and number of microcracks, while stiffness is mainly affected by accumulation of cracks and
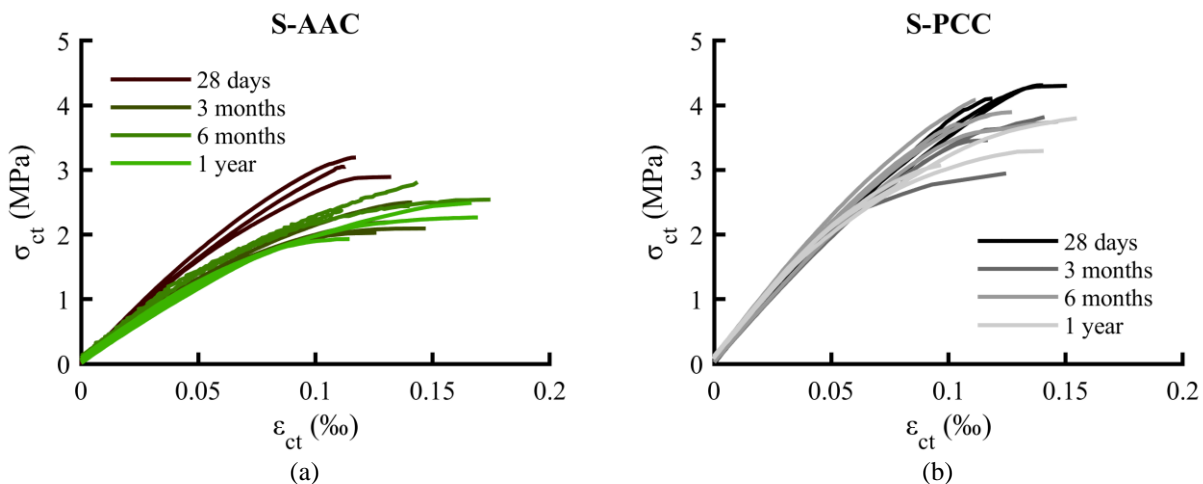

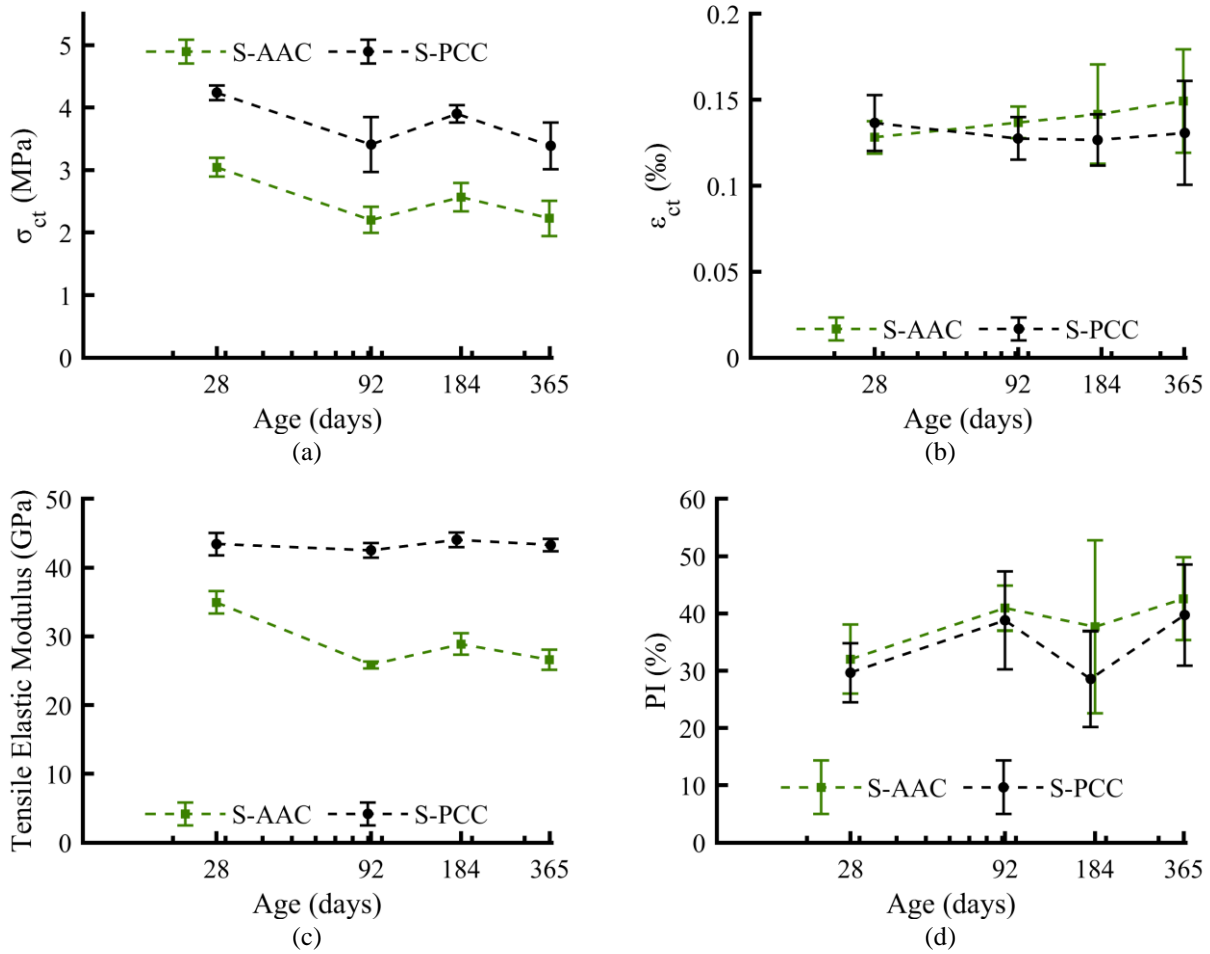**Figure 3**: Tensile stress-strain behavior for (a) S-AAC and (b) S-PCC

4

Figure 4: Development of (a) mean tensile strength, (b) strain capacity, (c) tensile elastic modulus and (d) plasticity index over time

crack width.

Unlike S-PCC, S-AAC shows a significant decrease in elastic modulus over time (Figure 4c), indicating that pre-existing microcracks could be wider in S-AAC than in S-PCC. Similar decreases have been observed before for the compressive elastic modulus of GGBFS-based AACs exposed to drying [13, 14].

Nevertheless, S-AAC exhibits similar plasticity as S-PCC, as can be depicted from the plasticity index in Figure 4d. Furthermore, both concretes show that the mean plasticity tends to increase over time, indicating that the uniformity of the stress distribution decreases due the accumulation of microcracks. Note, as the plasticity index is determined from the elastic modulus, peak stress and peak strain (**Eq. (2)**), the scatter of these properties is propagated in the plasticity index. This limits the analysis of plasticity to tendencies of mean values only.

3.2 Fracture behavior

Due to the brittle nature of concrete and energy release upon fracturing, it is challenging to obtain stabilized post-peak behavior in uniaxial tensile tests [22, 40]. In particular for S-PCC it was difficult to obtain stabilized post-peak behavior. None of the samples tested at 28 days led to a stable crack opening, possibly due to high tensile strength and brittleness of S-PCC. Nevertheless, it was possible to observe some tendencies in the fracture behavior for different concrete types and testing ages.

Figure 5 shows the stress-crack opening behavior for S-AAC and S-PCC. This figure shows that both concretes are capable of
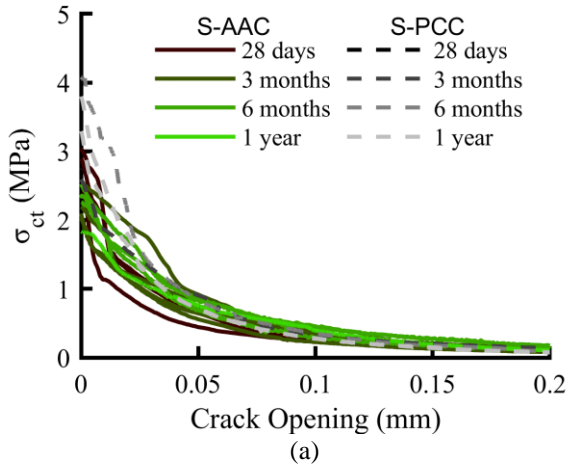
5

Figure 5: Stress – crack opening behavior of S-AAC and S-PCC over time.

transferring small stresses beyond 0.2 mm crack opening. A similar observation has been

made by Hordijk [22], who attributed the transfer of stresses at larger crack openings to friction of interlocked aggregates, which is among other factors dependent on the tortuosity of the fracture plane. Figure 6 shows typical fracture planes for S-AAC and S-PCC. Both concretes show similar fracture planes with the fracture plane passing mainly around aggregates. Although this was anticipated for S-PCC, which is known to have an interfacial transition zone (ITZ) with higher porosity than its matrix, GGBFS-based AACs have been characterized as a dense and homogenous material without a distinguishable more porous ITZ [41, 42]. A possible explanation for the fracture plane to pass around aggregates in S-AAC could be the formation of microcracks in S-AAC, weakening the ITZ and matrix.
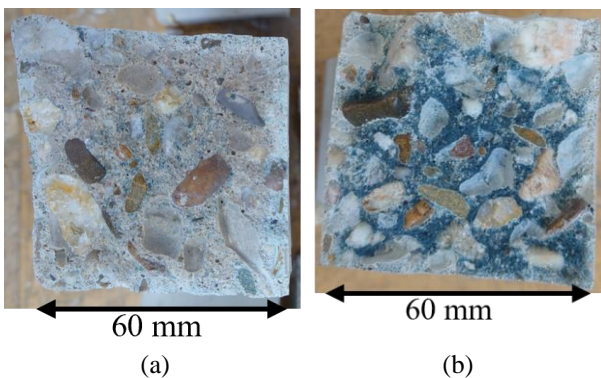

Figure 6: Fracture plane of (a) S-AAC and (b) S-PCC.

The descending branch of S-AAC becomes more gradual over time, while for S-PCC the descending branch becomes steeper at later ages. This could indicate that S-AAC softens over time, while S-PCC becomes more brittle. Similarly, the characteristic length (Figure 7a), an indicator for brittleness, rapidly increases for S-AAC over time, while it decreases for S-PCC. Note, the characteristic length is determined from tensile strength, stiffness and fracture energy and is therefore influenced by the effect of drying on these properties. A decrease in characteristic length indicates more brittleness. A decreasing characteristic length under drying for CEMI-based concretes has been observed before [22] and was related to the reduction in moisture content under drying: namely the strength then increases [43]. However, the tensile strength decreases for both concretes in the current study. Unlike S-PCC, S-AAC showed a significant decrease in elastic modulus over time (Figure 4), contributing to an increasing characteristic length. Furthermore, both concretes show a similar development of fracture energy over time (Figure 7b). As fracture energy is significantly impacted by tensile strength, the temporary increase in fracture energy from 3 months to 6 months might be related to the partial recovery of tensile strength (Figure 4). Similarly, the decrease in fracture energy from 6 months to 1 year is in line with the long-term strength reduction for both concretes. Interestingly, despite the lower tensile strength of S-AAC, similar fracture energies are obtained for the studied concretes over time, indicating that S-AAC softens more significantly than S-PCC under drying.

In the current study, brittleness of concrete has been evaluated by a plasticity index and its characteristic length. According to both methods, S-AAC indicates to be less brittle than S-PCC. However, another common definition to describe the brittleness of a material is by the ratio of tensile and compressive strength. When adopting this definition, S-AAC is, due to its lower tensile strength, more brittle than S-PCC, which is how AACs are commonly defined in literature [17, 44]. Hence, one should be careful by choosing an appropriate method and linking
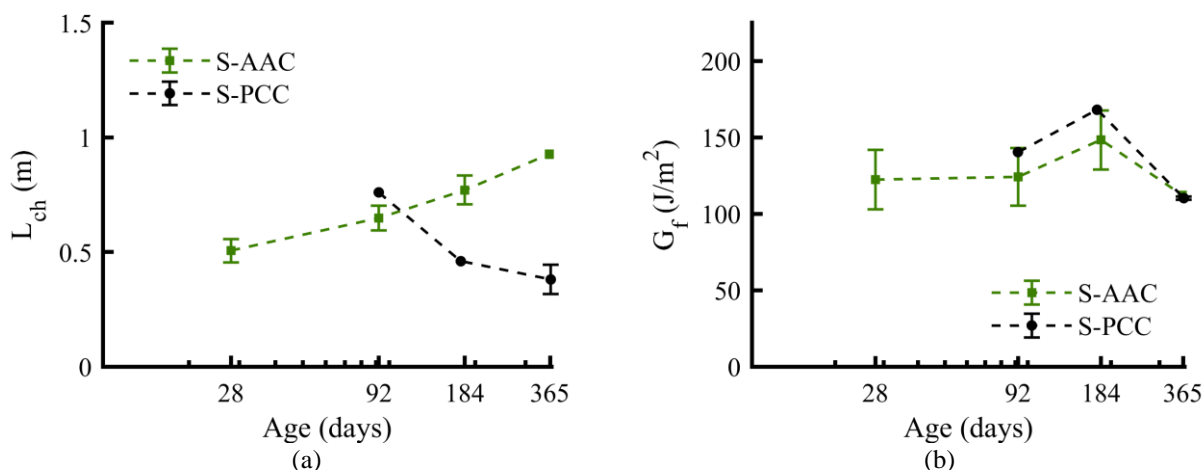
Figure 7: Development of (a) characteristic length and (b) fracture energy over time.

it with underlying fracture mechanisms for evaluating new materials.

4 CONCLUSION

Tensile behavior of a GGBFS-based AAC was investigated under direct tension at different testing ages and was compared to a CEMIII/B-based concrete. Tensile stress-strain and stress-crack opening behavior have been analyzed and mechanical properties, such as tensile strength, tensile elastic modulus, strain capacity and fracture energy have been used to determine the brittleness of AAC over time. The following conclusions can be drawn:

1) GGBFS-based AAC exhibits lower tensile strength compared to a CEMIII/B-based concrete at all testing ages.
2) Under drying, both concretes show reduced long-term tensile strength. After 6 months, strength continued to decrease, indicating that long-term strength reductions are not temporary and eigen stresses could cause concrete microcracking.
3) Unlike CEMIII/B-based concrete, GGBFS-based AAC showed significant reductions in its tensile elastic modulus under drying.
4) Both concretes showed increasing plasticity index over time, indicating that the uniformity of the stress distribution reduced over time. This could possibly be an effect of microcracking.

5) GGBFS-based AAC showed an increase in characteristic length over time, while it decreased for CEMIII/B-based concrete. A decreasing characteristic length indicates that the material becomes more brittle. Note, characteristic length is influenced by tensile strength, elastic modulus and fracture energy. Whereas both concretes yielded similar fracture energies, tensile strength and elastic modulus of GGBFS-based AAC were significantly lower than that of CEMIII/B-based concrete at all testing ages.
6) Similar fracture planes were obtained for GGBFS-based AAC and CEMIII/B-based concrete, with their fracture planes passing around aggregates. This indicates that also in GGBFS-based AACs an ITZ that is weaker than its matrix is developed.

It is important to note that the current study focused on a specific GGBFS-based AAC and compares the results with a CEM III/B-based concrete under specific curing (>95% RH) and exposure conditions (55% RH and 20ºC). Adopting a different alkaline activator, type of binder and/or exposure environment might lead to different results. Therefore, it is encouraged to focus on different curing regimes, binder compositions, activators and exposure conditions in future studies. The experimental work of the current study helps understand the long-term behavior of GGBFS-based AACs.

Future studies will focus on modelling the long-term engineering properties of GGBFS-based AACs.

REFERENCES

[1] D.N. Huntzinger, T.D. Eatmon, A life-cycle assessment of Portland cement manufacturing: comparing the traditional process with alternative technologies, *Journal of Cleaner Production* 17(7) (2009) 668-675.

[2] S.A. Miller, A. Horvath, P.J.M. Monteiro, Readily implementable techniques can cut annual CO2-emissions from the production of concrete by over 20%, *Environmental Research Letters* 11(7) (2016).

[3] K.L. Scrivener, R.J. Kirkpatrick, Innovation in use and research on cementitious material, *Cement and Concrete Research* 38(2) (2008) 128-136.

[4] IEA, Technology Roadmap - Low-Carbon Transition in the Cement Industry, IEA, Paris, 2018.

[5] K.-H. Yang, J.-K. Song, K.-I. Song, Assessment of CO2 reduction of alkali-activated concrete, J*ournal of Cleaner Production* 39 (2013) 265-272.

[6] S. Fernando, C. Gunasekara, D.W. Law, M.C.M. Nasvi, S. Setunge, R. Dissanayake, M.G.M.U. Ismail, Long-Term Mechanical Properties of Blended Fly Ash—Rice Husk Ash Alkali-Activated Concrete, *ACI Materials Journal* 119(5) (2022).

[7] A. Wardhono, C. Gunasekara, D.W. Law, S. Setunge, Comparison of long term performance between alkali activated slag and fly ash geopolymer concretes, *Construction and Building Materials* 143 (2017) 272-279.

[8] C.H. Un, J.G. Sanjayan, R. San Nicolas, J.S.J. van Deventer, Predictions of long-term deflection of geopolymer concrete beams, *Construction and Building Materials* 94 (2015) 10-19.

[9] A.M. Humad, J.L. Provis, K. Habermehl-Cwirzen, M. Rajczakowska, A. Cwirzen, Creep and Long-Term Properties of Alkali-Activated Swedish-Slag Concrete, *Journal of Materials in Civil Engineering* 33(2) (2021).

[10] F.G. Collins, J.G. Sanjayan, Microcracking and strength development of alkali activated slag concrete, *Cement and Concrete Composites* 23 (2001) 345-352.

[11] F.G. Collins, J.G. Sanjayan, Workability and mechanical properties of alkali activated slag concrete, *Cement and Concrete Research* 29 (1999) 455-458.

[12] Z. Li, S. Zhang, X. Liang, G. Ye, Cracking potential of alkali-activated slag and fly ash concrete subjected to restrained autogenous shrinkage, *Cement and Concrete Composites* 114 (2020).

[13] S. Prinsse, D.A. Hordijk, G. Ye, P. Lagendijk, M. Luković, Time-dependent material properties and reinforced beams behavior of two alkali-activated types of concrete, *Structural Concrete* 21(2) (2019) 642-658.

[14] H.J. Bezemer, N. Awasthy, M. Lukovic, Multiscale Analysis of Long-term Mechanical and Durability Behaviour of Two Alkali-activated Slag-based Types of Concrete, *Construction and Building Materials* 407 (2023).

[15] M. Nedeljkovic, Z. Li, G. Ye, Setting, Strength, and Autogenous Shrinkage of Alkali-Activated Fly Ash and Slag Pastes: Effect of Slag Content, *Materials* 11(11) (2018).

[16] I. Ismail, S.A. Bernal, J.L. Provis, S. Hamdan, J.S.J. van Deventer, Drying-induced changes in the structure of alkali-activated pastes, *Journal of Materials Science* 48(9) (2013) 3566-3577.

[17] R.J. Thomas, S. Peethamparan, Alkali-activated concrete: Engineering properties and stress–strain behavior, *Construction and Building Materials* 93 (2015) 49-56.

[18] N.A. Farhan, M.N. Sheikh, M.N.S. Hadi, Investigation of engineering properties of normal and high strength fly ash based geopolymer and alkali-activated slag concrete compared to ordinary Portland cement concrete, *Construction and Building Materials* 196 (2019) 26-42.

[19] K.-H. Yang, A.-R. Cho, J.-K. Song, Effect of water–binder ratio on the mechanical properties of calcium hydroxide-based alkali-activated slag concrete, *Construction and Building Materials* 29 (2012) 504-511.

[20] H. Wang, L. Wang, L. Li, B. Cheng, Y. Zhang, Y. Wei, The Study on the Whole

Stress-Strain Curves of Coral Fly Ash-Slag Alkali-Activated Concrete under Uniaxial Compression, *Materials (Basel)* 13(19) (2020).

[21] NEN, Testing hardened concrete - Part 3: Compressive strength of test specimens, NEN-EN 12390-3:2019, European Committee for Standardization, Brussels, 2019.

[22] D. Hordijk, Local approach to fatigue of concrete [dissertation], Delft University of Technology, Delft, 1991.

[23] J.S.o.C. Engineers, Recommendations for Design and Construction of High Performance Fiber Reinforced Cement Composites with Multiple Fine Cracks (HPFRCC), 2018.

[24] D.J. Cook, P. Chindaprasirt, Influence of loading history upon the tensile properties of concrete, *Magazine of Concrete Research* 33(116) (1981) 154-160.

[25] NEN, Testing hardened concrete - Part 13: Determination of secant modulus of elasticity in compression, NEN-EN 12390-13:2021, European Committee for Standardization, Brussels, 2021.

[26] V. Hucka, B. Das, Brittleness Determination of Rocks by Different Methods, *International Journal of Rock Mechanics and Mining Sciences & Geomechanics Abstracts* 11 (1974) 389-392.

[27] P. Petersson, Crack growth and development of fracture zones in plain concrete and similar materials [dissertation], Division of Building Materials, Lund Institute of Technology, Lund, 1981.

[28] N.K. Lee, H.K. Lee, Setting and mechanical properties of alkali-activated fly ash/slag concrete manufactured at room temperature, *Construction and Building Materials* 47 (2013) 1201-1209.

[29] Z. Li, B. Delsaute, T. Lu, A. Kostiuchenko, S. Staquet, G. Ye, A comparative study on the mechanical properties, autogenous shrinkage and cracking proneness of alkali-activated concrete and ordinary Portland cement concrete, *Construction and Building Materials* 292 (2021).

[30] Z. Li, X. Liang, C. Liu, M. Liang, K. van Breugel, G. Ye, Thermal deformation and stress of alkali-activated slag concrete under semi-adiabatic condition: Experiments and simulations, *Cement and Concrete Research* 159 (2022).

[31] Z. Li, T. Lu, Y. Chen, B. Wu, G. Ye, Prediction of the autogenous shrinkage and microcracking of alkali-activated slag and fly ash concrete, *Cement and Concrete Composites* 117 (2021).

[32] H. Ye, A. Radlińska, Shrinkage mechanisms of alkali-activated slag, *Cement and Concrete Research* 88 (2016) 126-135.

[33] J. Ma, F. Dehn, Shrinkage and creep behavior of an alkali-activated slag concrete, *Structural Concrete* 18(5) (2017) 801-810.

[34] N. Awasthy, E. Schlangen, D. Hordijk, B. Šavija, M. Luković, The role of eigen-stresses on apparent strength and stiffness of normal, high strength, and ultra-high performance fibre reinforced concrete, *Developments in the Built Environment* 16 (2023).

[35] J. Bonzel, Einfluss der Nachbehandlung und des Feuchtigkeitszustands auf die Zugfestigkeit des Betons, *Betontechnische Berichte 1970* (1970) 99-132.

[36] I. Maruyama, H. Sasano, Y. Nishioka, G. Igarashi, Strength and Young's modulus change in concrete due to long-term drying and heating up to 90°C, *Cement and Concrete Research* 66 (2014) 48-63.

[37] H. Sasano, I. Maruyama, Mechanism of drying-induced change in the physical properties of concrete: A mesoscale simulation study, *Cement and Concrete Research* 143 (2021).

[38] M. Lin, M. Itoh, I. Maruyama, Mechanism of Change in Splitting Tensile Strength of Concrete during Heating or Drying up to 90°C, *Journal of Advanced Concrete Technology* 13(2) (2015) 94-102.

[39] H.W. Reinhardt, Factors affecting the tensile properties of concrete, in: J. Weerheijm (Ed.), Understanding the Tensile Properties of Concrete, In Woodhead Publishing Series in Civil and Structural Engineering 2013, pp. 19-51.

[40] J.G.M.v. Mier, Concrete Fracture a multiscale approach [doctoral dissertation], Delft University of Technology, 2013.

[41] S.A. Bernal, R. Mejía de Gutiérrez, A.L. Pedraza, J.L. Provis, E.D. Rodriguez, S. Delvasto, Effect of binder content on the

performance of alkali-activated slag concretes, *Cement and Concrete Research* 41(1) (2011) 1-8.

[42] Y. Ding, J.-G. Dai, C.-J. Shi, Mechanical properties of alkali-activated concrete: A state-of-the-art review, *Construction and Building Materials* 127 (2016) 68-79.

[43] F.H. Wittmann, F. Sun, T. Zhao, Strength and fracture energy of concrete in seawater., *In Proceedings of the Fracture Mechanics of Concrete and Concrete Structures* (FraMCoS6), Catania, Italy, 2007, pp. 17-22.

[44] C. Duran Atiş, C. Bilim, Ö. Çelik, O. Karahan, Influence of activator on the strength and drying shrinkage of alkali-activated slag mortar, *Construction and Building Materials* 23(1) (2009) 548-555.